metals

MDPI

Article

Mechanical Properties of Refined A356 Alloy in Response to Continuous Rheological Extruded Al-5Ti-0.6C-1.0Ce Alloy Prepared at Different Temperatures

Da Teng [1,2], Guangzong Zhang [1,2,*], Shuo Zhang [1,2], Junwen Li [1,2] and Renguo Guan [1,2]

[1] Key Laboratory of Near-Net Forming of Light Metals of Liaoning Province, Dalian Jiaotong University, Dalian 116028, China; dateng120812@163.com (D.T.); zhangsh_vip@163.com (S.Z.); joelee0527@163.com (J.L.); guanrenguo@sina.cn (R.G.)

[2] Engineering Research Center of Continuous Extrusion, Ministry of Education, Dalian Jiaotong University, Dalian 116028, China

* Correspondence: gzzhang@djtu.edu.cn

Abstract: The microstructure is an important factor determining the mechanical properties of A356 alloy. In this experiment, the refiner Al-5Ti-0.6C-1.0Ce master alloys under different preparation temperatures were prepared, and the A356 alloy was refined. The effects of preparation temperature on the number and morphological distribution of each phase in Al-Ti-C-Ce master alloy and the effects of Al-Ti-C-Ce master alloy at different preparation temperatures on the microstructure and mechanical properties of A356 alloy were explored successively. Results showed that, as preparation temperature increased from 850 to 1150 °C, $TiAl_3$ changed from large blocks to long strips and a needle-like phase, and $Ti_2Al_{20}Ce$ changed from a bright white block to a broken small block phase. Al-5Ti-0.6C-1.0Ce prepared at 1050 °C can significantly refine the α-Al of A356 alloy and modify eutectic Si. The α-Al grain size was refined from about 1540 to 179.7 μm, and the eutectic Si length was refined from about 22.3 to 17.8 μm with the transition from a coarse needle-like to a short rod-like structure. The ultimate tensile strength and elongation of A356 alloy changed non-monotonically, and the peak values were 282.216 MPa and 3.9% with the Al-Ti-C-Ce preparation temperature of 1050 °C and 950 °C, respectively.

Keywords: Al-5Ti-0.6C-1.0Ce; preparation temperature; grain refinement; eutectic Si modification; mechanical properties

check for updates

Citation: Teng, D.; Zhang, G.; Zhang, S.; Li, J.; Guan, R. Mechanical Properties of Refined A356 Alloy in Response to Continuous Rheological Extruded Al-5Ti-0.6C-1.0Ce Alloy Prepared at Different Temperatures. *Metals* **2023**, *13*, 1344. https://doi.org/10.3390/met13081344

Academic Editor: Sergei Alexandrov

Received: 27 June 2023
Revised: 16 July 2023
Accepted: 24 July 2023
Published: 27 July 2023

Copyright: © 2023 by the authors. Licensee MDPI, Basel, Switzerland. This article is an open access article distributed under the terms and conditions of the Creative Commons Attribution (CC BY) license (https://creativecommons.org/licenses/by/4.0/).

1. Introduction

The Al-Si alloy is widely used in the aviation, aerospace, and automotive industries due to its excellent casting properties and high mechanical properties [1–3]. The A356 alloy, as a typical Al-Si alloy, has received extensive attention for its mechanical properties. It has been confirmed that the microstructure of the A356 alloy prepared by the conventional casting process is usually composed of an α-Al matrix and needle-like eutectic Si [4–6]. The grain size of α-Al, the shape and distribution of eutectic Si, and the number of secondary phases such as Mg_2Si [7] are important factors determining the alloy properties. However, premature crack sprouting and tensile fracture due to the formation of needle-like eutectic Si and tearing of the α-Al matrix reduce the strength and elongation of the alloy, limiting applications in the industry [8,9]. Therefore, grain refinement is a necessary goal for high-performance aluminum alloys. In modern industrial production, there are mainly the following grain refinement technologies, such as chemical incubation [10], rapid solidification [11], and external solidification [12–15], among which chemical incubation is currently the most widely used. The addition of grain refiners has become a common practice to control grain nucleation and growth, which not only improves the alloy strength but also helps to improve the toughness [16,17]. Al-Ti-based master alloys (i.e., Al-Ti,

Al-Ti-B) refine the A356 alloy to improve its mechanical properties. Moreover, the addition of trace elements such as Na can change the eutectic Si morphology from a needle-like to a fibrous structure. Mallapura [18] studied the effect of the addition of an Al-Ti-based grain refiner on the microstructure and properties of forged A356 alloy. The results show that the dual effects of forging and a grain refiner can make the grain more refined, but it does not explain the role of the grain refiner. Therefore, it is necessary to explore the role of the grain refiner in cast A356 and the influence of different variables on the effect of the grain refiner. Moreover, the addition of chemical elements still has some drawbacks [19]. For example, due to the agglomeration of boride particles, the Al-Ti-based master alloy (Al-Ti, Al-Ti-B) will occur a 'poisoning phenomenon', leading to microstructure local roughness and seriously reducing the refinement. Also, Na and other elements severely burn during the casting process so that the modification effect is greatly reduced. Al-Ti-C can avoid the degradation of refinement effect caused by boride agglomeration, and TiC particles have 'poisoning immunity' to Cr, Zr, and other elements, so it is considered the most promising grain refiner. However, considering the poor wettability of graphite and aluminum melt, carbon and aluminum melt need to react above 1150 °C; it is difficult for graphite to react with aluminum melt to generate TiC particles [20]. Rare earth elements, known as 'flavor elements', have a great potential to refine the grains of aluminum alloys and to modify eutectic Si [21]. In recent years, the unique chemical activity and surface adsorption properties of single or mixed rare earth elements have been recognized by researchers, and they have been combined with Al-Ti-based grain refiners during the refinement of Al-Si alloys [22–24]. Certain amounts of Sc and Eu can significantly refine the primary α-Al phase, modify eutectic Si, and improve the mechanical properties of A356 alloys, but the application is limited due to the high costs [25–27]. The Ce element has special activity and can significantly refine grain size and improve eutectic Si modification when added to the alloy, which in the aluminum melt exists in the form of a surface-active element [28]. In the solidification process, the Ce element can enrich the solid–liquid interface front and inhibit the growth of the grain. Simultaneously, the Ce element is enriched in the interstices of the dendrites, causing subcooling of the composition and further broken dendrite, which refines the grains [29–32]. Moreover, the Ce element is the surface active substance that improves the wettability of the aluminum melt to the second phase [33]. Due to its unique electronic structure and electronegativity difference, the Ce element has a strong affinity with an oxygen atom (Ce 1.12, Al 1.61, O 3.44, Pauling scale), which easily breaks the oxide film barrier and provides favorable interface conditions for the reaction between C and Al [34–37]. However, the combination of rare earth elements and Al-Ti-based grain refiners to prepare new high-efficiency grain refiners has seldom been studied. Therefore, in this paper, Ce was combined with an Al-Ti-C grain refiner, and a more efficient grain refiner was prepared by continuous rheological extrusion technology.

In this work, CRE Al-5Ti-0.6C-1.0Ce master alloys were prepared by fluorine salt method at different preparation temperatures. The effect of preparation temperature on the morphology and distribution of the phases in the CRE Al-5Ti-0.6C-1.0Ce master alloy was investigated. The reasons for the influence of preparation temperature on the morphology of each phase in A356 alloy were revealed, and it was found that when the preparation temperature reached 1050 °C, the nucleation rate of the TiC phase increased significantly, and the morphology of $Ti_2Al_{20}Ce$ changed significantly. The effect of master phases on grain refinement in the A356 alloy and the mechanism of Ce influence on the eutectic Si modification of the A356 alloy were revealed. The current work will provide a new idea for the preparation of a double-effect intermediate alloy with grain refinement and eutectic Si modification.

2. Materials and Methods

2.1. Materials

This experiment includes the preparation of the refiner Al-Ti-C-Ce alloy by continuous rheological extrusion at different temperatures and the refinement of the A356 alloy by the

Al-Ti-C-Ce alloy. The main materials were high-purity aluminum (99.95%), carbon powder, K_2TiF_6 (99.99%), Al-20Ce, and A356 alloy. The compositions of the prepared Al-Ti-C-Ce alloy at different temperatures are shown in Table 1.

Table 1. Chemical compositions of refiner Al-5Ti-0.6C-1.0Ce (wt.%).

Grain Refiner	Temperature (°C)	Ti (%)	C (%)	Ce (%)	Al
Al-5Ti-0.6C-1.0Ce	850 (M1)	4.98	0.58	1.06	Bal.
	950 (M2)	4.86	0.59	1.13	Bal.
	1050 (M3)	5.07	0.65	1.04	Bal.
	1150 (M4)	4.87	0.62	1.22	Bal.

The experimental process is shown in Figure 1. Firstly, the high-purity aluminum was melted in the resistance furnace, and when the temperature reached 850 °C, the Al-20Ce alloy was added and held for 30 min. Then, the fluorine salt method was used to add a carbon powder and K_2TiF_6 mixture to reach a certain temperature (850, 950, 1050, and 1150 °C), and the reaction rate was accelerated by manual stirring with a titanium rod during holding for 30 min. Then, the salts on the melt surface were removed, and CH_2Cl_6 was added for degassing. Finally, the melt was poured into the continuous rheological extrusion (CRE) cross-sectional wheel, as shown in Figure 1a, to obtain Al-5Ti-0.6C-1.0Ce master alloys prepared at four temperatures, defined as M1, M2, M3, and M4, respectively. The phase compositions were analyzed by X-ray diffractometer (XRD, Panalytical Empyrean, London, UK), and the microstructure was examined by scanning electron microscopy (SEM, Zeiss Ultra Plus, Munich, Germany) equipped with energy-dispersive spectroscopy (EDS) detectors.

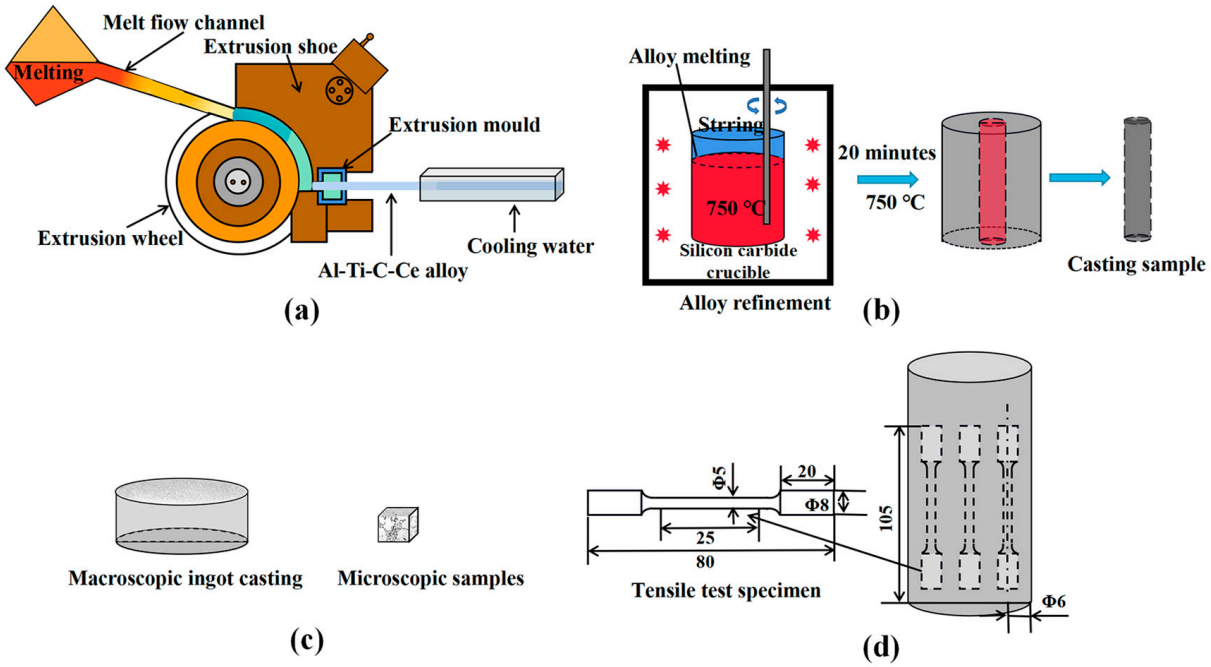

Figure 1. Schematic diagram of the experimental process and mold. (**a**) Al-Ti-C-Ce CRE process. (**b**) Refinement of A356 alloy. (**c**) Macro ingot and micro samples. (**d**) Stretch rod sample and sampling location.

Secondly, the A356 alloy was immersed into the graphite crucible and melted in a resistance furnace (SG-5-12A-220V, Φ 200 × 250, HengTai Electric Furnace Inc., Wei Fang, China). When the temperature of the molten metal reaches 750 °C, M1, M2, M3, and M4 refiners are added, respectively, and the addition amount is 0.2 wt.%. Then, the melt was held for 20 min, and after degassing and deslagging, the melt was poured into the

preheated disk shape and cylindrical molds. Samples of 10 × 10 × 10 mm were taken from the preheated disk shape, as shown in Figure 1c, which were put into a resistance furnace and heated at 540 °C for 4 h. Then, samples were quickly removed from the resistance furnace and placed in cold water, cooled to 20 °C. Next, samples were dried and heated to 170 °C for 5 h. Finally, the samples were removed from the oven and cooled to room temperature. Subsequently, the samples were ground, polished, and etched with a Keller reagent (95% H_2O, 2.5% HNO_3, 1.5% HCl, 1.0% HF). Microstructure analysis was performed using SEM (Zeiss Ultra Plus, Munich, Germany). The average grain size of the sample was observed using a metallographic microscope (OM, Leica DMi8 A, Weztlar, Germany) and evaluated using the image analysis software IPP (Image Pro, Media Cybernetics, Silver Spring, MD, USA). The refinement effect of the refiner Al-Ti-C-Ce master alloys prepared at different temperatures on the A356 alloy was compared.

2.2. Sample Testing and Characterization

According to the GB/T228.1-2010 tensile test standard, the dimension of the tensile test specimen is Φ 5 × 25 mm, as shown in Figure 1d. The temperature tensile test was performed with an electronic universal testing machine (Shimadzu AG-IC 100 kN, Kyoto, Japan) at a constant tensile rate of 1.0 mm/min, and three specimens were measured to ensure experimental accuracy. Post-tension experiments were performed to observe the fracture morphology using SEM.

3. Result and Discussion

3.1. Refinement Effect of Master Alloys with Different Preparation Temperatures

Figure 2 shows the macro- and micro-structures of the A356 alloy under different refiners, where Figure 2a–e shows the macrostructure of the original A356 alloy and alloys under the addition of M1, M2, M3, and M4, respectively. Figure 2f–j show the microstructure accordingly. From the macroscopic structure of α-Al in Figure 2, it can be seen that the introduction of the Al-Ti-C-Ce master alloy effectively reduces the grain size, and due to the different preparation temperatures, the refinement effect of M1, M2, M3, and M4 is different. As shown in Figure 2a, the unrefined A356 alloy has large columnar particles in the center and small block-like particles on the outer surface with an average particle size of 1540 μm. As shown in Figure 2b,c, after adding the CRE Al-Ti-C-Ce master alloys of M1 and M2, the block-like particles still exist in the matrix. After adding the CRE Al-Ti-C-Ce alloy of M3, the block-like particles disappear and are replaced by fine and uniform particles. By further increasing the preparation temperature, the refined A356 again shows block-like particles, and the refinement effect is reduced, as shown in Figure 2e.

Figure 3 shows the average grain size of the A356 alloy without and with the addition of refiners M1, M2, M3, and M4. According to the GB/T 6394-2002 metal average grain size determination method, the average grain size is calculated by the linear intercept method. The refinement effects in the A356 alloy by refiners M1, M2, M3, and M4 are different. Higher or lower preparation temperatures will both affect the grain refinement. The grain size of Figure 3 shows a non-monotonic relationship with the preparation temperature of M1, M2, M3, and M4. Under the same addition, the average grain size of refined A356 alloy by M1, M2, M3, and M4 is 214.9, 189.5, 179.7, and 214.8 μm, respectively. The CRE Al-Ti-C-Ce master alloy obtains the best refinement effect on A356 at the preparation temperature of 1050 °C. In order to clarify the underlying mechanism, the second phases in Al-Ti-C-Ce master alloys are further investigated.

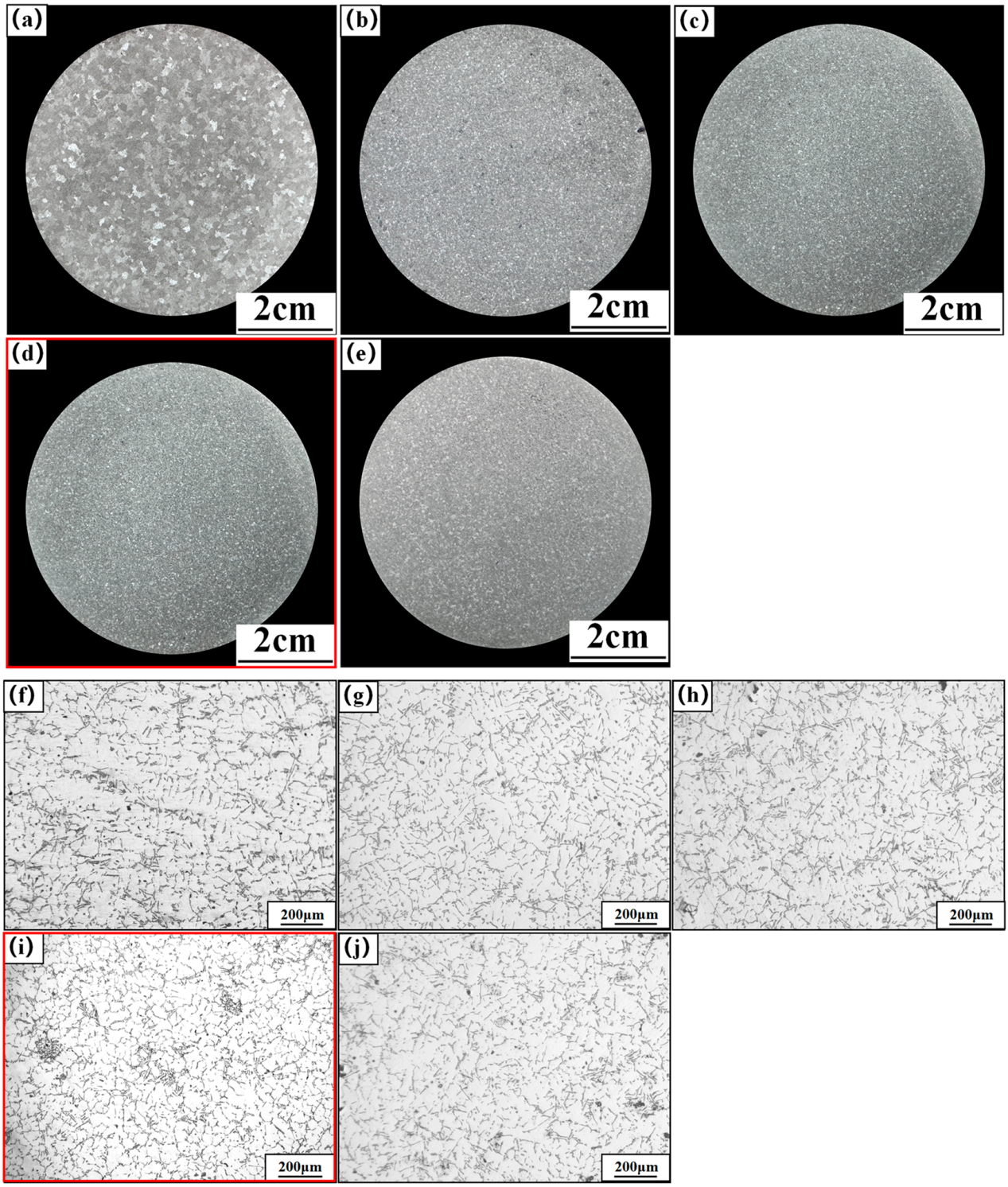

Figure 2. Macro- and micro-structure of refined A356 alloy by the continuous rheological extrusion (CRE) Al-Ti-C-Ce alloy with different preparation temperatures. (**a**,**f**) Unrefined, (**b**,**g**) 850 °C, (**c**,**h**) 950 °C, (**d**,**i**) 1050 °C, (**e**,**j**) 1150 °C.

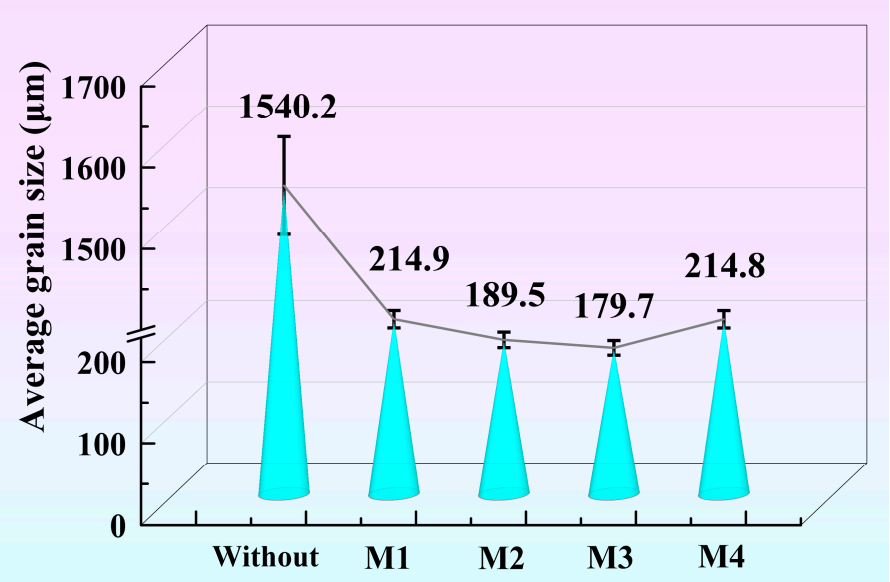

Figure 3. Grain size of A356 alloy without and with the addition of refiners M1 (850 °C), M2 (950 °C), M3 (1050 °C), and M4 (1150 °C).

3.2. Effect of Temperature Change on Al-Ti-C-Ce Microstructure

Figure 4 shows XRD patterns of M1, M2, M3, and M4 alloys. The main phases include α-Al, $TiAl_3$, TiC, and $Ti_2Al_{20}Ce$. Moreover, the diffraction peaks of TiC and $Ti_2Al_{20}Ce$ at 1050 °C are significantly higher than those at other temperatures. It reflects that more nucleated particles generate at this temperature, corresponding to grain size in Figure 3.

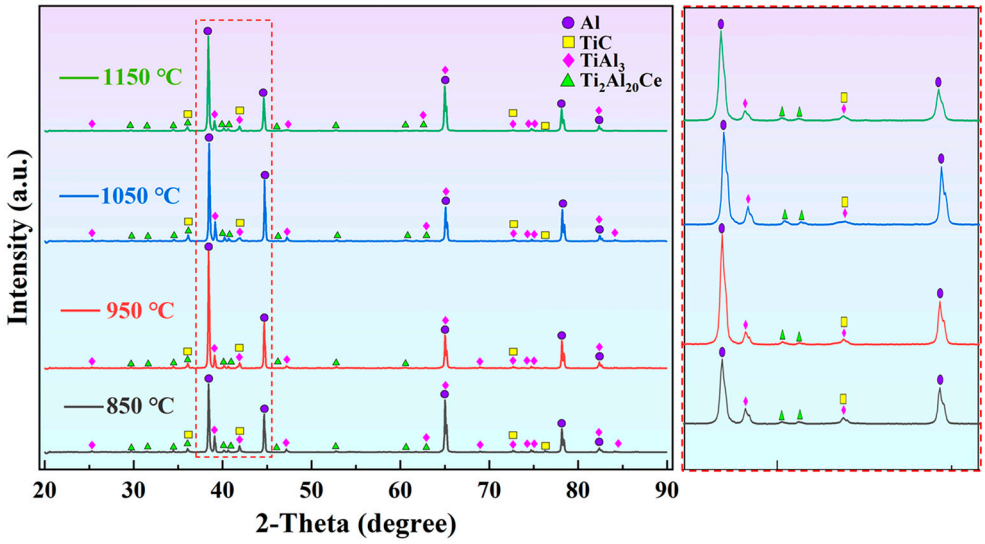

Figure 4. XRD patterns of Al-5Ti-0.6C-1Ce alloys at different preparation temperatures.

Figure 5 shows the microstructures of M1, M2, M3, and M4. From Figure 5a, it can be seen that massive phases are distributed in the gray aluminum matrix, most of which are light gray, and a few are bright white. Also, there are a small number of particle phases aggregated at the grain boundaries; both the light gray and white block phases have certain fragmentation phenomena. Combined with EDS results of points A, B, and C in Figure 5f–h, the light gray, bright white large, and fine particles are determined as $TiAl_3$, $Ti_2Al_{20}Ce$, and TiC phases, respectively. With the increasing preparation temperature, the morphology of the $TiAl_3$ phase changes obviously. It can be found from Figure 5a–d at preparation temperatures of 850 and 950 °C, the $TiAl_3$ phase presents as a light gray block. When the temperature reaches 1050 °C, it exists in both blocks and long strips. As the temperature

reaches 1150 °C, it becomes long strips and needle-like. Also, the morphology of $Ti_2Al_{20}Ce$ depends on the preparation temperature, i.e., a higher preparation temperature induces a smaller size. According to the mapping of Al, Ti, and Ce elements in Figure 5, a small part of the $Ti_2Al_{20}Ce$ phase and $TiAl_3$ are intersected with each other, signifying the formation connection between the two phases.

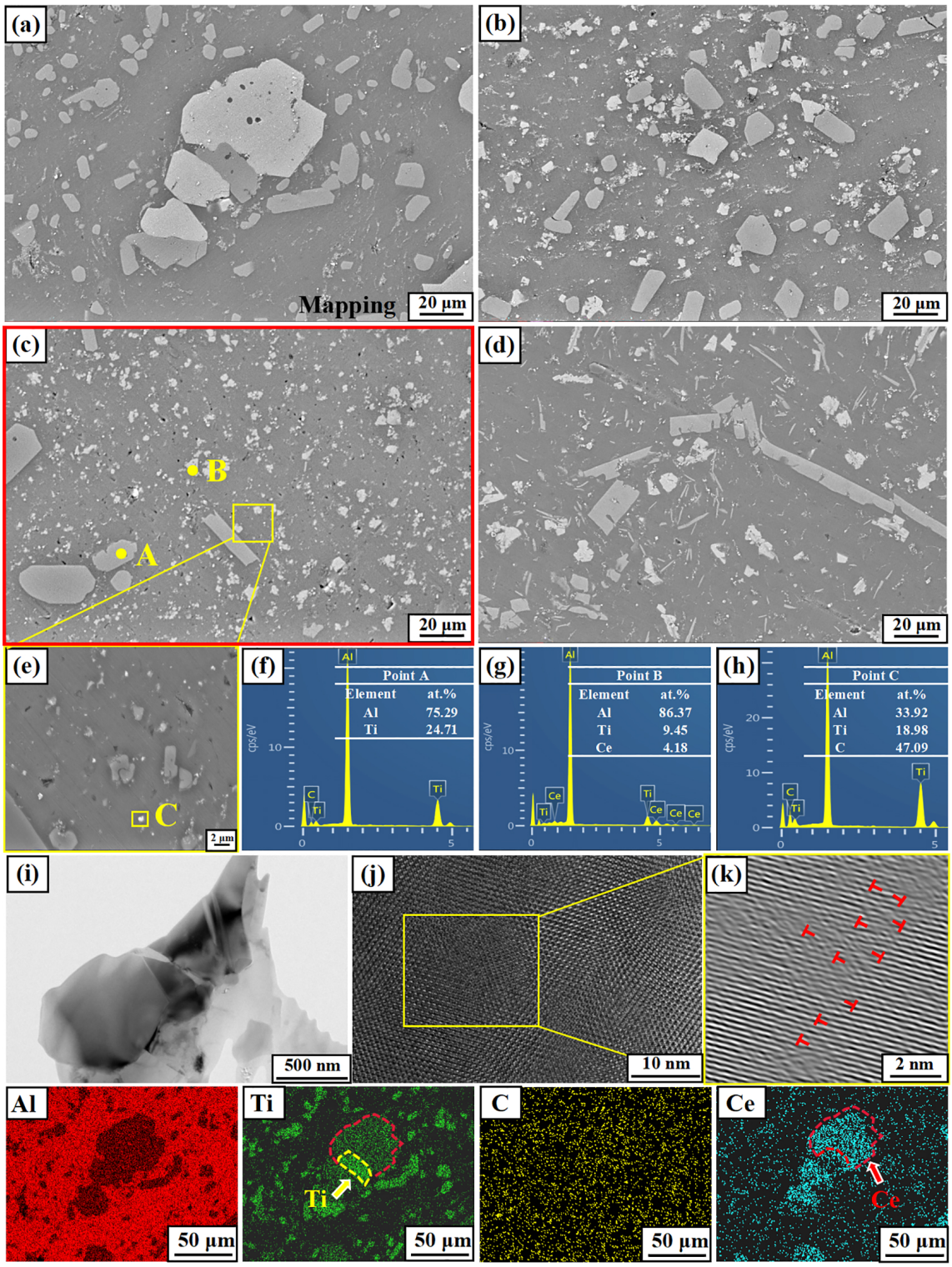

Figure 5. SEM images of Al-Ti-C-Ce refiner alloy with different preparation temperatures. (**a**) M1, (**b**) M2, (**c**,**e**) M3, (**d**) M4, (**f**–**h**) EDS result of points A, B, and C, respectively. (**i**–**k**) TEM image of the $Ti_2Al_{20}Ce$.

According to the mapping of Ti and Ce in Figure 5, it can be seen that Ti and Ce have a certain transition zone; that is, the Ti-Ce layer is generated. In addition, Figure 5i shows the warping structure described above. Abundant dislocations, marked by the symbol ⊥, were identified near the interface between $TiAl_3$ and $Ti_2Al_{20}Ce$, as shown in Figure 5k. According to the dislocation density formula:

$$\rho = \frac{L}{V} \tag{1}$$

V is the crystal volume, L is the total length of the dislocation line. Due to the increase in the preparation temperature, the size of the $Ti_2Al_{20}Ce$ phase becomes smaller, and the number increases, resulting in an increase in the total length of the dislocation line and an increase in the dislocation density, as shown in Figure 5k.

The rare-earth element Ce is a surface-active substance. The addition of rare earth element Ce to the aluminum melt not only generates $Ti_2Al_{20}Ce$ particles but also makes the wettability between graphite and aluminum melt better and reduces TiC particle aggregation. Comparing Figure 5a–d, the distribution of the TiC phase becomes more uniform with the preparation temperature increasing from 850 to 1050 °C. Due to the solute redistribution of $TiAl_3$, Ti is enriched on the surface of $TiAl_3$ and reacts with C to form a new TiC phase, leading to the cluster phenomenon at 1150 °C, which reduces the effect of grain refinement. As shown in Figure 5g, there is a certain amount of $TiAl_3$ phase around the fine TiC particles, which is the same as the phenomenon described by the dual nucleation theory, i.e., $TiAl_3$ is generated again on the TiC surface and becomes a heterogeneous nucleation core. Moreover, the introduction of rare earth Ce has also promoted the formation of TiC. McCartney [38] also shows a simplified expression of the nucleation rate of TiC precipitated from a liquid alloy:

$$I = CN_V^P \exp\left[\frac{-16\pi\sigma_\alpha f(\theta)}{3k_B\Delta S^2\Delta T^2}\right] \tag{2}$$

C is the coefficient relevant to atomic diffusion, N_V^P is the number of embryos per unit volume of the melt, σ_α is the liquid-solid interfacial tension, $f(\theta)$ is the wetting angle factor, k_B is the Boltzmann constant, ΔS is the nucleation entropy, and ΔT is the degree of nucleation undercooling. Due to the introduction of surfactant Ce, the entropy (ΔS) will increase, and at the same time, the atomic diffusion rate (C) is promoted. Moreover, with the preparation temperature increases, the wetting angle between TiC and the melt becomes smaller, and according to Equation (2), it can be seen that with the decrease of the wetting angle, the nucleation rate of TiC gradually increases, promoting the formation of more TiC particles. This corresponds to the above TiC phase distribution being more uniform as the temperature rises. Based on the above factors, the nucleation rate of TiC increases, which promotes the refinement of grains.

3.3. Effect of Heat Treatment and Ce on Eutectic Silicon Morphology

Figure 6 shows the microstructure of eutectic Si without and with M1, M2, M3, and M4 alloy addition in the as-cast and T6 heat treatment states. The eutectic Si in the original as-cast A356 alloy shows a rough and plate-like morphology. Moreover, after the T6 heat treatment, the plate-eutectic Si phase is disrupted to form needles or rounded rod-like structure, as seen in Figure 7, but the length of the plate-eutectic Si phase is not changed, as shown in Figure 6a,b. When a certain amount of Al-Ti-C-Ce master alloy is added, taking the M3 addition as an example, a large number of short-plate eutectic Si appears, and long-plate eutectic Si appears to be broken. After the T6 heat treatment, the eutectic Si particles are clearly spherical and uniformly distributed, as shown in Figure 6g,h. Therefore, it can be inferred that the Al-Ti-C-Ce master alloys prepared at different preparation temperatures have a certain modification effect on the eutectic Si. Also, the heat treatment changes the morphology of the eutectic Si.

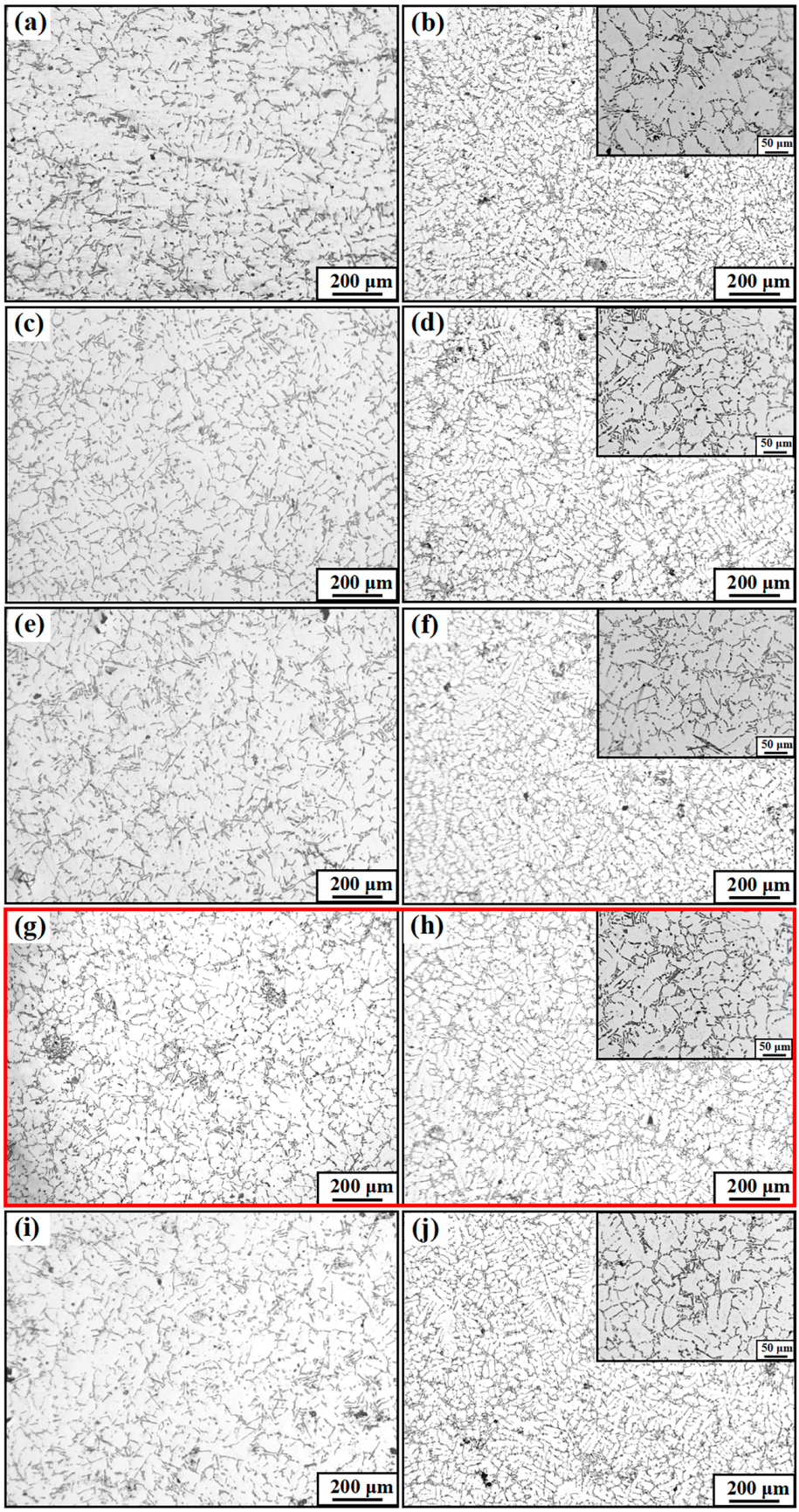

Figure 6. Microstructure images of A356 alloy in different states. (**a**) As-cast A356; (**c**,**e**,**g**,**i**) As-cast A356 with M1, M2, M3, M4 addition, respectively; (**b**) T6-A356; (**d**,**f**,**h**,**j**) T6-A356 with M1, M2, M3, and M4 addition, respectively.

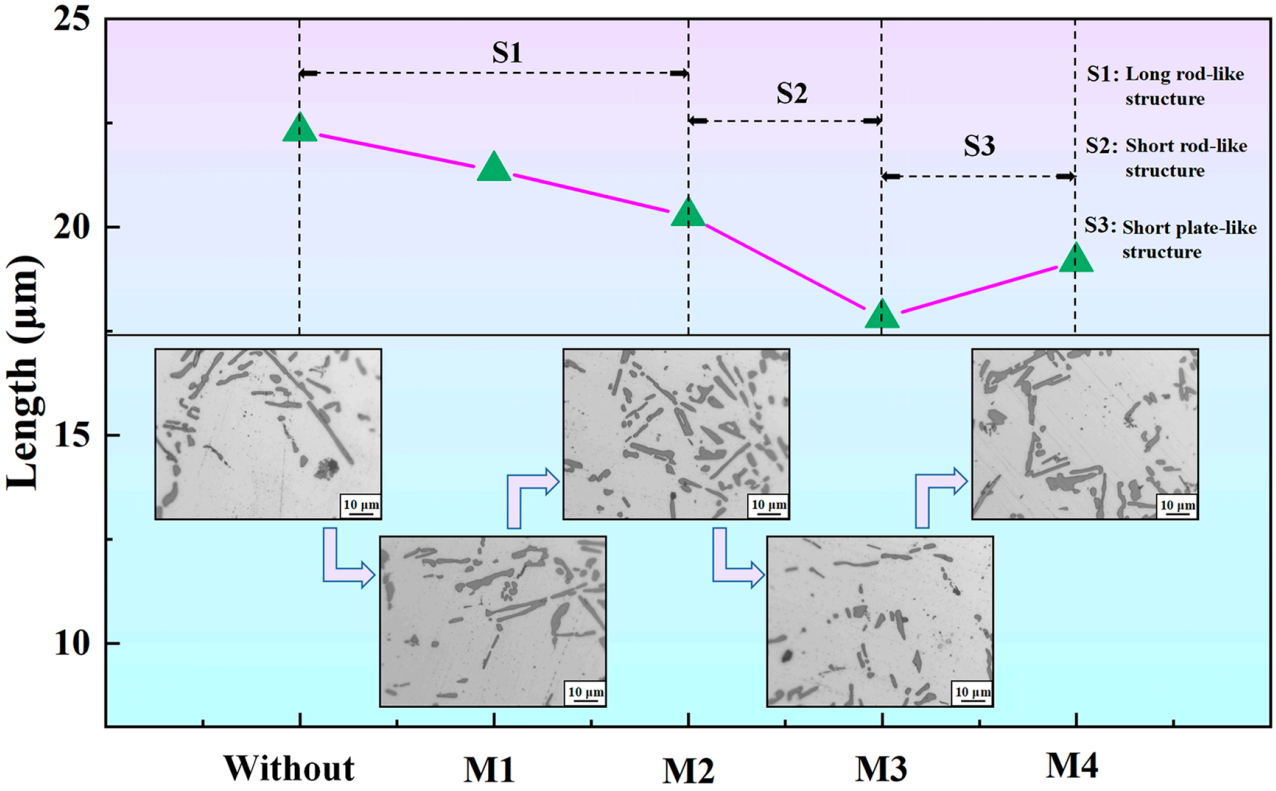

Figure 7. Length of eutectic Si in the T6-A356 alloys without and with M1, M2, M3, and M4 additions.

Figure 7 shows the length of eutectic Si in T6-A356 alloys. The apparent length of eutectic Si is automatically processed by OM digital images, and the length is counted by IPP software. The apparent length of eutectic Si particles inherits the original length, presenting a non-monotonic evolution. It is 22.3, 21.4, 20.3, 17.8, and 19.17 μm, respectively, for the alloys and obtains the peak value under M3 addition. According to the S1 stage in Figure 7, eutectic Si is predominantly long rod-like when M1 and M2 are added. In the S2 stage, due to the addition of M3, eutectic Si significantly modifies and becomes short rod-like. However, the length of eutectic Si grows rapidly again after the addition of M4.

Figure 8 shows the typical phase morphology of the A356 alloy without and with the addition of M3. Based on the element distributions and the ratios of points A to G, the light gray fishbone and needle-like phases in the matrix alloys is identified as α-AlFeSi and AlFeSiCe, respectively. It can be found from Figure 8b that, with the addition of M3, the fishbone shape will disappear, and a broken AlFeSiCe phase identified as point D will appear in the A356 alloy. Also, as reported by Wang [39], the Ce element can react with the AlFeSi phase to form a new broken AlFeSiCe phase. Compared with the α-AlFeSi phase, the newly formed AlFeSiCe phase is broken, which reduces the stress concentration during the tensile process and greatly improves the mechanical properties of A356. Furthermore, the eutectic Si in A356 shows a more broken morphology after the addition of M3, and the Ce element in Figure 8b is distributed around the eutectic Si. According to the change of eutectic Si morphology in Figure 8a,b, the Ce element in the alloy is free and can be distributed around the eutectic Si to hinder the growth and eventually form broken eutectic silicon.

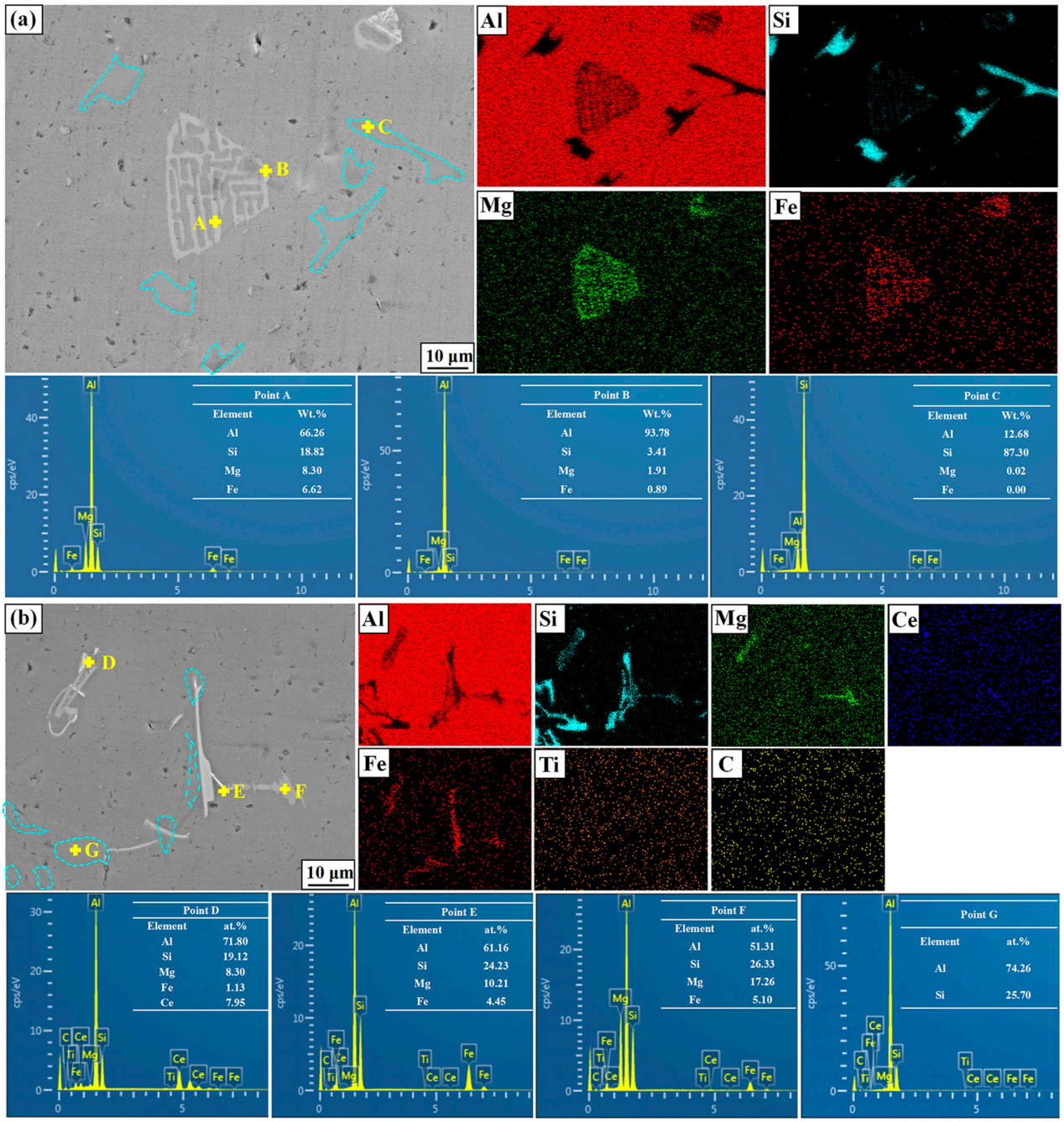

Figure 8. SEM images of A356 without and with M3 addition (**a**) without (**b**) with M3 addition.

Figure 9 shows the tensile strength and elongation of the T6-A356 alloy with the M1, M2, M3, and M4 additions. As the preparation temperature increases, the ultimate tensile strength and elongation both tend to increase and then decrease, but the temperature corresponding to the peak value is different. The peak tensile strength is obtained at the preparation temperature of 1050 °C, and the tensile strength and elongation are 282.2 MPa and 3.5%, respectively, while that for peak elongation is 950 °C, and the tensile strength and elongation are 262.9 MPa and 3.9%, accordingly. When the preparation temperature is further increased, the ultimate tensile strength and elongation of A356 alloy both decrease. Curry [40] gives the critical stress expression for coarse needle-like phases to break:

$$\sigma = \sqrt{\frac{\pi E Y_S}{2(1-V^2)L}} \tag{3}$$

where Y_S is the surface fracture energy per unit area, V is the Poisson's ratio, L is the length of the coarse phase, and E is the modulus of elasticity.

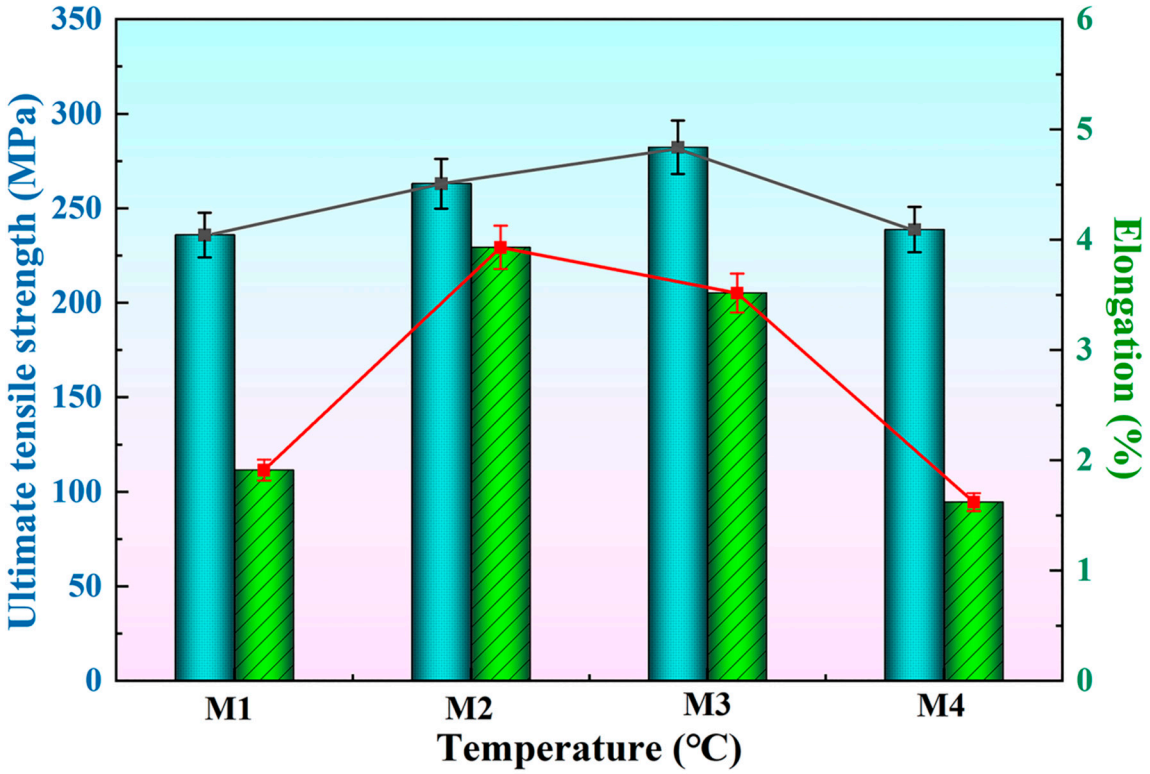

Figure 9. Tensile strength and elongation of T6-A356 alloy with the M1, M2, M3, and M4 additions.

According to Equation (3), the longer the size of coarse needle-like phases, the smaller the critical stress at break. This confirms the relationship between the length of eutectic silicon in Figure 7 and the tensile strength in Figure 9. The tensile strength of A356 alloy is determined by a variety of factors, including grain size and length of other coarse phases. With the introduction of Al-Ti-C-Ce master alloys, the size of α-Al grains and eutectic Si become smaller, the AlFeSi phase is transformed into the AlFeSiCe phase, and the tensile strength of the alloy gradually increases. However, when the preparation temperature is increased to 1150 °C, the needle-like eutectic Si appears, which reduces the mechanical properties.

Figure 10 shows the surface fracture morphology from tensile tests of the T6-A356 alloy with the M1, M2, M3, and M4 refiner additions. As shown in Figure 10a,e, the fracture of the A356 alloy with M1 addition is characterized by clear cleavage planes and tearing edges, which is typical of a brittle fracture. The A356 alloy consists of coarse α-Al dendrites and plate-like eutectic Si, which leads to premature cracking due to stress concentration. When M2 is added, the number of cleavage planes is reduced, but that of tendon fossas is increased, presenting as the ductile fracture in Figure 10b,f. Comparing Figure 10e–h, the number of tendon fossa is the most in Figure 10f, signifying the highest elongation of the A356 alloy with M2 addition. It can be seen from Figure 10g that when M3 is added, a large number of torn edges and tendon fossa exist in the fracture, but the number of tendon fossa is less than that in Figure 10f. For M4 addition, the fracture of Figure 10h is similar to that of Figure 10g, but the more tearing edges have a significant effect on the alloy mechanical properties, which keeps a good accordance with the results in Figure 9.

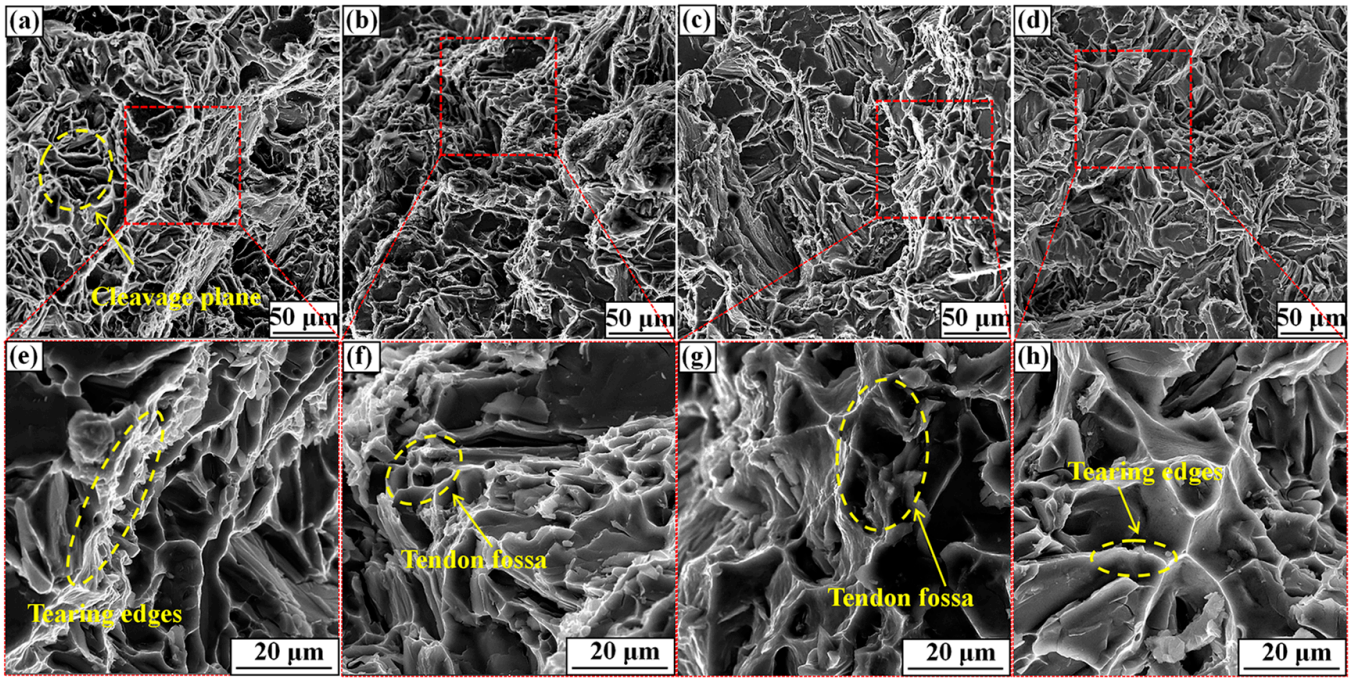

Figure 10. Tensile test surface fractures of T6-A356 alloy with the M1, M2, M3, and M4 refiner additions. (**a**,**e**) M1; (**b**,**f**) M2; (**c**,**g**) M3; (**d**,**h**) M4.

4. Conclusions

In this paper, a new Al-Ti-C-Ce grain refiner alloy was prepared, and the effect of which with different preparation temperatures on the microstructure and mechanical properties of A356 alloy was investigated. The following conclusions were drawn:

1. With the increasing preparation temperature, the $TiAl_3$ phase in the Al-Ti-C-Ce master alloy changed from blocks to a long strip; the $Ti_2Al_{20}Ce$ phase changed from the large blocks to the smaller ones, combined with the more uniform distribution of the TiC phase. The morphology of the refinement phase is changed, and the distribution is more uniform, which can provide more nucleation sites for α-Al and promote the grain refinement of the A356 alloy;
2. As the preparation temperature of Al-Ti-C-Ce increased, the grain size and eutectic Si length of A356 alloy decreased first and then increased. The peak grain size and eutectic length were 179.7 and 17.82 μm, respectively, at the preparation temperature of 1050 °C;
3. The Al-Ti-C-Ce grain refiner addition can significantly improve the mechanical properties of the A356 alloy. With the increase of preparation temperature, the ultimate tensile strength and elongation of A356 alloy changed non-monotonically, and the peak values were 282.216 MPa and 3.9% at Al-Ti-C-Ce preparation temperatures of 1050 °C and 950 °C, respectively. In addition, the preparation of the grain refiner by CRE technology provides a new idea for the coupling of a subsequent grain refiner and continuous rheological extrusion on A356.

Author Contributions: D.T., conceptualization, methodology, formal analysis, investigation, data curation, writing—original draft. G.Z., investigation, data curation, writing—review and editing, funding acquisition, supervision. S.Z. and J.L., validation, writing—review and editing. R.G., conceptualization, project administration, funding acquisition, supervision. All authors have read and agreed to the published version of the manuscript.

Funding: This work was supported by the National Key Research and Development Program of China [grant No. 2022YFE0137900, 2022YFB3706801], the Dalian High-level Talents Innovation Support Program [grant No. 2021RD06], the National Natural Science Foundation of China [grant No. U2241232], the Applied Basic Research Program of Liaoning Province [grant No. 2022JH2/101300003], and the National Natural Science Foundation of Liaoning Province [grant No. 2022-BS-262].

Data Availability Statement: The data that has been used is confidential.

Acknowledgments: The authors wish to acknowledge Guangzong Zhang for support with experimental facilities and preparation. The authors also sincerely thank Shuo Zhang for the technical support provided.

Conflicts of Interest: The authors declare no conflict of interest.

References

1. Jiao, X.Y.; Liu, C.F.; Guo, Z.P.; Tong, G.D.; Ma, S.L.; Bi, Y.; Zhang, Y.F.; Xiong, S.M. The characterization of Fe-rich phases in a high-pressure die cast hypoeutectic aluminum-silicon alloy. *J. Mater. Sci. Technol.* **2020**, *51*, 54–62.
2. Jiang, J.F.; Liu, Y.Z.; Xiao, G.F.; Wang, Y.; Xiao, X.Q. Effects of Temperature and Time on Microstructural Evolution of Semisolid 5A06 Aluminum Alloy: Preparation of Semisolid Billets in Ellipsoid Solid Phase. *J. Mater. Eng. Perform.* **2020**, *29*, 5346–5359.
3. Limmaneevichitr, C. Fading mechanism of grain refinement of aluminum-silicon alloy with Al-Ti-B grain refiners. *Mater. Sci. Eng. A* **2003**, *349*, 197–206.
4. Hanieh, A.; Salman, N.; Rooholllah, J. Effects of Ti particles and T6 heat treatment on the microstructure and mechanical properties of A356 alloy fabricated by compocasting. *Mater. Sci. Eng. A* **2021**, *818*, 141443.
5. Zhang, Y.; Ji, S.; Fan, Z. Improvement of mechanical properties of Al-Si alloy with effective grain refinement by in-situ integrated Al-2.2Ti-1B-Mg refiner. *J. Alloys Compd.* **2017**, *710*, 166–171.
6. Tang, P.; Li, W.F.; Wang, K.; Du, J.; Chen, X.Y.; Zhao, Y.J.; Li, W.Z. Effect of Al-Ti-C master alloy addition on microstructures and mechanical properties of cast eutectic Al-Si-Fe-Cu alloy. *Mater. Des.* **2017**, *115*, 147–157.
7. Ding, W.W.; Chen, T.L.; Zhao, X.Y.; Xu, C.; Tang, X.C.; Qiao, J.S. Effect of CeO_2 on Microstructure and Synthesis Mechanism of Al-Ti-C Alloy. *Materials* **2018**, *11*, 2508.
8. Lakshmi, R.N.; Rainer, H. Rapid solidification of hypoeutectic aluminum copper alloys using fast-scanning calorimetry. *J. Alloys Compd.* **2022**, *925*, 166829.
9. Wang, J.H.; Zhu, J.Q.; Liu, Y.; Peng, H.P.; Su, X.P. Effect of spheroidization of eutectic Si on mechanical properties of eutectic Al-Si alloys. *J. Mater. Res.* **2018**, *33*, 1773–1781.
10. Zhang, L.; Zhou, W.; Hu, P.H.; Zhou, Q. Effect of Al-3Nb-1B Master Alloy on the Grain Refinement of AZ91D Magnesium Alloy. *Metall. Mater. Trans. B* **2016**, *47*, 1999–2004.
11. Wang, H.F.; An, Y.K.; Xu, X.; Guo, X.; Hu, Y. Rapid solidification microstructure evolution and grain refinement of deeply undercooled nickel alloys. *Mater. Charact.* **2020**, *170*, 110703. [CrossRef]
12. Liu, X.F.; Zhang, Z.G.; Gao, Z.; Bian, X.F. The influence of electromagnetic stirring on Al-Ti-B master alloys. *JOM* **2000**, *52*, 47–48.
13. Zhao, J.T.; Wu, X.Y.; Ning, L.P.; Zhang, J.J.; Han, C.; Li, Y.L. Wetting of aluminium and carbon interface during preparation of Al-Ti-C grain refiner under ultrasonic field. *Ultrason. Sonochem.* **2021**, *76*, 105633. [CrossRef] [PubMed]
14. Liu, Z.W.; Rakita, M.; Xu, W.; Wang, X.M.; Han, Q.Y. Ultrasound assisted combustion synthesis of TiC in Al-Ti-C system. *Ultrason. Sonochem.* **2015**, *27*, 631–637. [CrossRef] [PubMed]
15. Han, Y.F.; Li, K.; Wang, J.; Shu, D.; Sun, B.D. Influence of high-intensity ultrasound on grain refining performance of Al-5Ti-1B master alloy on aluminium. *Mater. Sci. Eng. A* **2005**, *405*, 306–312. [CrossRef]
16. Birol, Y. The performance of Al-Ti-C grain refiners in twin-roll casting of aluminium foilstock. *J. Alloys Compd.* **2007**, *430*, 179–187. [CrossRef]
17. Ma, X.G.; Liu, X.F.; Ding, H.M. A united refinement technology for commercial pure Al by Al-10Ti and Al-Ti-C master alloys. *J. Alloys Compd.* **2009**, *471*, 56–59. [CrossRef]
18. Mallapura, D.G.; Rajendra Udupaa, K.; Korib, S.A. Studies on the influence of grain refining and modification on microstructure and mechanical properties of forged A356 alloy. *Mater. Sci. Eng. A.* **2011**, *528*, 4747–4752. [CrossRef]
19. Ding, H.M.; Liu, X.F.; Yu, L.N. Influence of zirconium on grain refining efficiency of Al-Ti-C master alloys. *J. Mater. Sci.* **2007**, *42*, 9817–9821. [CrossRef]
20. Birol, Y. Grain refining efficiency of Al-Ti-C alloys. *J. Alloys Compd.* **2006**, *422*, 128–131. [CrossRef]
21. Xu, C.X.; Liang, L.P.; Lu, B.F.; Zhang, J.S.; Liang, W. Effect of La on Microstructure and Grain-Refining Performance of Al-Ti-C Grain Refiner. *J. Rare Earths* **2006**, *24*, 596–601. [CrossRef]
22. Shi, W.X.; Gao, B.; Tu, G.F.; Li, S.W. Effect of Nd on microstructure and wear resistance of hypereutectic Al-20%Si alloy. *J. Alloys Compd.* **2010**, *508*, 480–485. [CrossRef]
23. Król, M.; Staszuk, M.; Mikuszewski, T.; Kuc, D. Refinement effect of RE in light weight Mg-Li-Al alloys. *J. Therm. Anal. Calorim.* **2018**, *134*, 333–341. [CrossRef]

24. Najafi, S.; Sheikhani, A.; Sabbaghian, M.; Nagy, P.; Fekete, K.; Gubicza, J. Modification of the Tensile Performance of an Extruded ZK60 Magnesium Alloy with the Addition of Rare Earth Elements. *Materials* **2023**, *16*, 2828. [CrossRef]
25. Li, J.H.; Ludwig, T.H.; Oberdorfer, B.; Schumacher, P. Solidification behaviour of Al-Si based alloys with controlled additions of Eu and P. *Int. J. Cast Met. Res.* **2018**, *31*, 319–331. [CrossRef]
26. Wu, X.F.; Wang, K.Y.; Wu, F.F.; Zhao, R.F.; Chen, M.H. Simultaneous grain refinement and eutectic Mg_2Si modification in hypoeutectic Al-11Mg_2Si alloys by Sc addition. *J. Alloys Compd.* **2019**, *791*, 402–410. [CrossRef]
27. Furukawa, M.; Utsunomiya, A.; Matsubara, K.; Horita, Z.; Langdon, T.G. Influence of magnesium on grain refinement and ductility in a dilute Al-Sc alloy. *Acta Mater.* **2001**, *49*, 3829–3838. [CrossRef]
28. Chai, Y.F.; He, C.; Jiang, B.; Fu, J.; Jiang, Z.T. Influence of minor Ce additions on the microstructure and mechanical properties of Mg-1.0Sn-0.6Ca alloy. *J. Mater. Sci. Technol.* **2020**, *37*, 26–37. [CrossRef]
29. Jin, H.N.; Sui, Y.D.; Yang, Y.; Jiang, Y.H.; Wang, Q.D. Effect of Ce content on the microstructure and mechanical properties of squeeze-cast Al-5Mg-2.2Si-0.6Mn alloys. *J. Mater. Res. Technol.* **2022**, *19*, 1798–1804. [CrossRef]
30. Ding, W.W.; Xia, T.D.; Zhao, W.J.; Xu, Y.T. Effect of Al-5Ti-C Master Alloy on the Microstructure and Mechanical Properties of Hypereutectic Al-20%Si Alloy. *Materials* **2014**, *7*, 1188–1200. [CrossRef] [PubMed]
31. Liao, Q.Y.; Hu, W.X.; Le, Q.C.; Chen, X.R.; Jiang, Y.C. Improvement of Yield Asymmetry and Enhancement of Mechanical Properties of Extruded AZ110 Alloy with La-Rich Misch Metal Addition. *Met. Mater. Int.* **2022**, *28*, 1143–1156. [CrossRef]
32. Sun, Y.; Hung, C.; Hebert, R.J.; Fennessy, C.; Tulyani, S.; Aindow, M. Eutectic microstructures in dilute Al-Ce and Al-Co alloys. *Mater. Charact.* **2019**, *154*, 269–276. [CrossRef]
33. Song, X.C.; YAN, H.; Zhang, X.J. Microstructure and mechanical properties of Al-7Si-0.7Mg alloy formed with an addition of (Pr+Ce). *J. Rare Earths* **2017**, *35*, 412–418. [CrossRef]
34. Wang, F.; Hu, M.L.; Liu, T.; Jiang, B.; Ji, Z.S. Microstructure of Al-Ti-C master alloy triggered by rare-earth Ce. *J. Mater. Res.* **2022**, *37*, 1486–1496. [CrossRef]
35. Huang, J.X.; Feng, L.; Li, C.; Huang, C.F.; Li, J.G.; Friedrich, B. Mechanism of Sc poisoning of Al-5Ti-1B grain refiner. *Scr. Mater.* **2020**, *180*, 88–92. [CrossRef]
36. Wang, B.; Liu, X.X.; Wang, J.S.; Li, Q.; Liu, K.L.; Zhang, M.S. Uncovering the effects of Ce and superheat temperature on Fe-rich intermetallic and microporosity formation in aluminum alloy. *Mater. Charact.* **2022**, *193*, 112226. [CrossRef]
37. Meng, C.C.; Su, C.C.; Liu, Z.K.; Liao, D.X.; Rong, X.C.; Li, Y.Z.; Tang, H.Q.; Wang, J.S. Synergistic Effect of RE (La, Er, Y, Ce) and Al-5Ti-B on the Microstructure and Mechanical Properties of 6111Aluminum Alloy. *Metals* **2023**, *13*, 606. [CrossRef]
38. McCartney, D.G. Grain refining of aluminium and its alloys using inoculants. *Int. Mater. Rev.* **1989**, *34*, 247–260. [CrossRef]
39. Wang, Y.F.; Liu, Q.; Yang, Z.; Yang, C.M.; Tan, K. Effffect of Ce Addition and Heat Treatment on Microstructure Evolution and Tensile Properties of Industrial A357 Cast Alloy. *Metals* **2020**, *10*, 1100. [CrossRef]
40. Curry, D.A.; Knott, J.F. Effect of microstructure on cleavage fracture toughness of quenched and tempered steels. *Met. Sci. J.* **1979**, *13*, 341–345. [CrossRef]

Disclaimer/Publisher's Note: The statements, opinions and data contained in all publications are solely those of the individual author(s) and contributor(s) and not of MDPI and/or the editor(s). MDPI and/or the editor(s) disclaim responsibility for any injury to people or property resulting from any ideas, methods, instructions or products referred to in the content.